

Comparative performance of some constitutive models in stress rotation

Published

25th November 2019

<https://doi.org/10.5802/ogeo.3>

Edited by

Ivo Herle

Institute of Geotechnical Engineering,
Technische Universität Dresden,
Germany

Reviewed by

David Mašín

Faculty of Science,
Charles University in Prague,
Czech Republic

X. S. Shi

Department of Civil and Environmental
Engineering, Hong Kong University of
Science and Technology,
Hong Kong, China

Correspondence

Fabian Schranz

Department of Engineering Science,
University of Oxford
Parks Road, Oxford, OX1 3PJ
United Kingdom

Fabian.Schranz@eng.ox.ac.uk

Unit of Geotechnical and Tunnel
Engineering, University of Innsbruck

**Fabian Schranz^{a, b}, Wolfgang Fellin^b
& Dimitrios Kolymbas^b**

^a Department of Engineering Science, University of Oxford

^b Unit of Geotechnical and Tunnel Engineering, University of Innsbruck.

Abstract. The dilatancy/contractancy of soil is of particular importance for compaction, consolidation, liquefaction, etc. Interestingly, constitutive relations are often unsatisfactory in modelling volume changes in the sense that their predictions deviate considerably from each other. This scatter is pronounced in problems with stress rotation. Therefore, in this paper some selected constitutive relations are investigated with respect to their performance at stress rotation. The obtained numerical simulations are compared with each other and also with experimental results from the $1\gamma 2\varepsilon$ and the hollow cylinder apparatuses.

Keywords. Principal stress rotation, Constitutive Model, Hypoplasticity, Barodesy, Sanisand



This article is licensed under the Creative Commons Attribution
NonCommercial ShareAlike 4.0 License.



Open Geomechanics is member of the
Centre Mersenne for Open Scientific Publishing

1. Introduction

Soil is often exposed to a rotation of the principal stress axes due to engineering work. For instance, in the case of a shallow foundation with only a vertical load the stress in the soil rotates (except at the symmetry axis). Furthermore, the subsoil of offshore platforms is exposed to rotation of the principal stress axes due to wave action, as Ishihara and Towhata [1983] showed. Another example is deep vibro-compaction. The vibroflot device implies a combination of compression and shear waves, Fellin [2000], which also induce principal stress rotations in the soil. As compaction is the main issue in this case, a material model used in a computation must predict volume changes due to principal stress rotations. Its effect on soil behaviour and the corresponding modelling have been investigated by Gutierrez and Ishihara [2000], Gutierrez et al. [1991a,b, 1993], Gutierrez and Vardoulakis [2007], Gutierrez and Wang [2009], Gutierrez et al. [2009], Pradel et al. [1990].

Conventional laboratory tests such as triaxial and oedometer tests are so-called rectilinear extensions and, hence, do not include rotation of principal stress axes. However, some special apparatuses imply rotation of the principal axes (e.g. the hollow cylinder apparatus, Ishihara and Towhata [1983], the directional shear cell by Arthur et al. [1980], or the $1\gamma 2\varepsilon$ apparatus by Joer et al. [1992]). In experiments with these apparatuses a volumetric change of the sample is observed, although the stress invariants remain constant.

Deformations induced by stress rotation can be calculated with advanced constitutive models. However, it turns out that the obtained results deviate from each other within a large range, although the models behave similarly in triaxial and even simple shear tests. Therefore, the simulation of deformations induced by stress rotation turns out to be important for the evaluation and verification of advanced constitutive models. In this paper, we perform numerical simulation of stress rotation using some selected constitutive models (elasto-plastic, hypoplastic and barodetic ones) and we compare the obtained results with results from the $1\gamma 2\varepsilon$ apparatus and from hollow cylinders.

2. Constitutive models

The following constitutive models are investigated: Hardening Soil with small-strain stiffness, Benz [2007] (HSS), Sanisand, Taiebat and Dafalias [2008], Hypoplasticity, Kolymbas [1985, 1991] in the formulation of von Wolfersdorff [1996] with and without the extension of Niemunis and Herle [1997] for intergranular strain (Hypo i.s.) and Barodesy, Kolymbas [2015].

2.1. Hardening Soil with small-strain stiffness

Hardening Soil is an elastoplastic constitutive relation with shear and compression hardening. It does not use the void ratio e as a state variable. Hence, it does not include the concept of critical state soil mechanics.

The model predicts a decreasing stiffness for initial loading, due to hardening. For a calculation starting from an isotropic state the yield surface coincides with the isotropic axis. With ongoing shearing the yield surface is inflated until it reaches the Mohr-Coulomb yield surface. In the case of unloading, as for the reloading, the response is elastic until the yield surface is reached again.

To realistically describe hydrostatic loading, the model uses a cap. The small-strain stiffness is introduced with a small-strain overlay into the model. For small-strain cycles the shear stiffness depends only on the strain history, whereas for larger strains it is stress-dependent.

2.2. Sanisand

Sanisand is an elastoplastic model that incorporates the concept of critical state soil mechanics and of bounding surface plasticity. It uses a narrow wedge that forms the yield surface and two further surfaces in the stress space. They define a limit surface for admissible stress states, as well as a dilatancy surface which determines the plastic strain rate.

The shape of these surfaces is the same as the critical state surface, however, their size depends on the actual void ratio. For dense soil (in the sense of critical state theory) the bounding surface in principal stress space comprises the critical state surface, and the dilatancy surface is nested therein. For loose samples the bounding surface is smaller, and the dilatancy surface is larger than the critical state surface. For critical states the bounding and dilatancy surfaces coincide with the critical one.

2.3. Hypoplasticity

Hypoplasticity uses a rate equation to calculate the objective stress rate $\dot{\mathbf{T}}$ and does not distinguish between elastic and plastic deformations. Hence, Hypoplasticity needs neither yield surface nor plastic potential. In general, Hypoplasticity can be written as

$$\dot{\mathbf{T}} = \mathbf{h}(\mathbf{T}, \mathbf{D}, \dots) = \mathcal{L} : \mathbf{D} + \mathbf{N} \|\mathbf{D}\| \quad . \quad (1)$$

Here, \mathcal{L} denotes a fourth-order tensor for the linear term and \mathbf{N} a second order tensor for the nonlinear term of the hypoplastic function \mathbf{h} . Due to the linear and the nonlinear terms, the stiffness for loading and unloading is different. The function \mathbf{h} is homogeneous of degree n in stress, \mathbf{T} , i.e. the stiffness is stress-dependent, and positive homogeneous of degree one in the rate of deformation, \mathbf{D} , i.e. Hypoplasticity is rate-independent. Furthermore, in all recent versions the void ratio e is an additional variable and this enables to incorporate the concepts of critical state soil mechanics.

2.4. Barodesy

Barodesy is a constitutive model recently introduced by Kolymbas [2012]. It is based on the asymptotic behaviour of soil and on critical state soil mechanics. Just like Hypoplasticity, Barodesy needs neither yield surface nor plastic potential and can be written as a single tensorial equation.

2.5. Calibration and comparison

To compare the different models initially various laboratory tests are computed: a drained triaxial test, a simple

Table 1. Material parameters of Sanisand for Toyoura Sand Taiebat and Dafalias [2008]

G_0	K_0	α_c^c	c	e_0	λ	ξ	n^d
125 kPa	150 kPa	1.2	0.712	0.934	0.019	0.7	2.1

A_d	n^b	h_0	c_h	p_r	ρ_c	θ	X
0.4	1.25	36.96	0.987	5.5 MPa	0.37	0.18	0.8

Table 2. Material parameters of Hardening Soil Small (calibrated for Toyoura Sand from Verdugo and Ishihara [1996])

E_{50}^{ref}	E_{oed}^{ref}	E_{ur}^{ref}	m	c	φ	ψ
30 MPa	30 MPa	120 MPa	0.6	0 kPa	33°	4°

ν_{ur}	p^{ref}	K_0^{nc}	R_f	$\sigma_{Tension}$	E_0^{ref}	$\gamma_{0.7}$
0.2	100 kPa	0.46	0.9	0 kPa	300 MPa	0.0002

Table 3. Material parameters of Hypoplasticity in the version of von Wolffersdorff, Herle [1997]

φ_c	h_s	n	e_{d0}	e_{c0}	e_{i0}	α	β
30°	2.6 GPa	0.27	0.61	0.98	1.10	0.18	1.00

Table 4. Material parameters of Barodesy (preliminary calibration for Toyoura Sand from Verdugo and Ishihara [1996])

φ_c	c_2	c_3	c_4	c_5	e_{c0}	e_{min}
30°	1.3	-1.5	2 MPa	40	0.93	0.55

shear test with constant volume and a simple shear test with constant normal stress are simulated with Toyoura sand by Verdugo and Ishihara [1996]. The material parameters for the calculation can be seen in Tables 1, 2, 3 and 4. For Sanisand and Hypoplasticity parameters from literature (Taiebat and Dafalias [2008] and Herle [1997]) are used. Hardening Soil and Barodesy are calibrated with results of a triaxial test from Verdugo and Ishihara [1996].

The consolidation pressure of the triaxial test is 100 kPa and the initial void ratio e_0 is 0.831. The results of the numerical computation can be seen in Figure 1. Taking into account the experimental scatter, Schwiteilo and Herle [2017], all models perform well.

In the simple shear test with constant volume the sample is loaded with a vertical load of 100 kPa, the lateral pressure is set to 50 kPa (which corresponds to a K_0 -state). The initial void ratio is the same as in the triaxial test ($e_0 = 0.831$). The stress evolution is shown in Fig. 2. The differences are more pronounced than for the drained triaxial test.

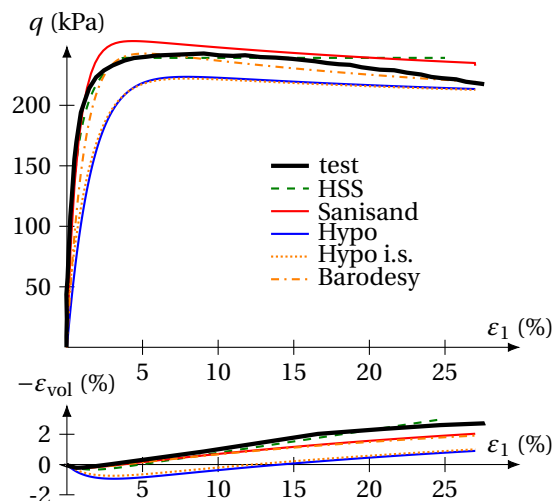


Figure 1. Stress-strain and volumetric strain curves for different constitutive models compared with a triaxial test in Verdugo and Ishihara [1996]

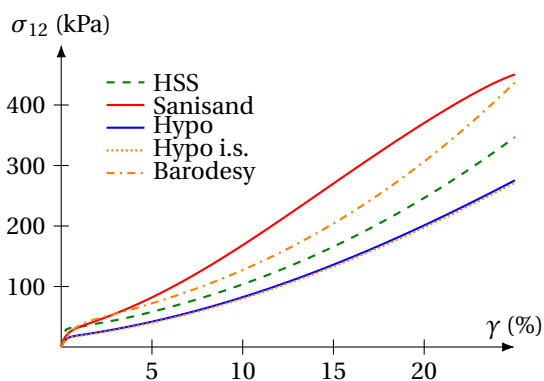


Figure 2. Stress-strain curves for a simple shear test with constant volume obtained with different constitutive models

For the simple shear with a constant vertical stress the initial conditions are the same as in the simple shear test with constant volume. In Fig. 3 the results of this test are shown. The differences of the stress are in the same order as in the drained triaxial test. Note that the volumetric changes almost coincide in this test.

3. Kinematic analysis of the deformations

The deformation is described by equations 2 using the functions $g(t)$ (in vertical direction) and $h(t)$ (in horizontal direction), while the shear deformation is described by $f(t)$, see Fig. 4. In the simulation of the principal stress rotation the out-of-plane normal stress σ_{33} is constant, and the strain in direction x_3 has to be calculated. The axial deformation in this direction is described by the function $d(t)$, Fig. 5. The other two shear deformations in the x_1 - x_3 and the x_2 - x_3 -planes are not of interest for the considered motion.

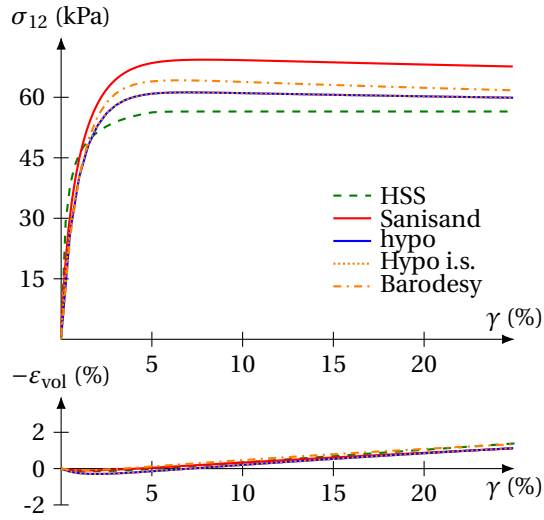


Figure 3. Stress-strain and volumetric strain curves for a simple shear test with constant normal stress obtained with different constitutive models

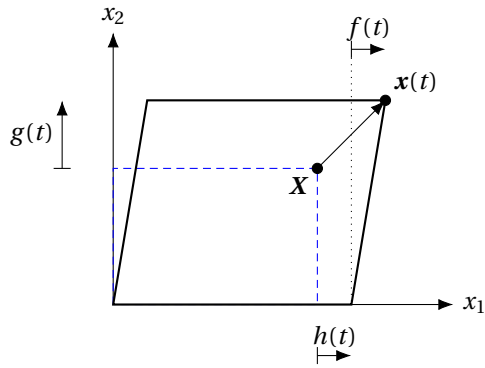


Figure 4. Deformation in two dimensions

A material point being at \mathbf{X} at $t = 0$ moves to the position $\mathbf{x}(t)$ with

$$\begin{aligned} x_1(t) &= X_1 + X_1 h(t) + X_2 f(t) \\ x_2(t) &= X_2 + X_2 g(t) \\ x_3(t) &= X_3 + X_3 d(t) \end{aligned} \quad (2)$$

The corresponding stretching tensor \mathbf{D} is obtained from

$$\mathbf{D} = \text{sym}(\nabla \dot{\mathbf{x}}) \quad (3)$$

and reads

$$\mathbf{D} = \begin{bmatrix} \frac{\dot{h}}{1+h} & \frac{\dot{f}(1+h) - \dot{h}f}{2(1+h)(1+g)} & 0 \\ \frac{\dot{f}(1+h) - \dot{h}f}{2(1+h)(1+g)} & \frac{\dot{g}}{1+g} & 0 \\ 0 & 0 & \frac{\dot{d}}{1+d} \end{bmatrix} \quad (4)$$

and the spin tensor \mathbf{W} is

$$\mathbf{W} = \begin{bmatrix} 0 & \frac{\dot{f}(1+h) - \dot{h}f}{2(1+h)(1+g)} & 0 \\ \frac{\dot{h}f - \dot{f}(1+h)}{2(1+h)(1+g)} & 0 & 0 \\ 0 & 0 & 0 \end{bmatrix} \quad (5)$$

The dot over a function denotes its time derivative.

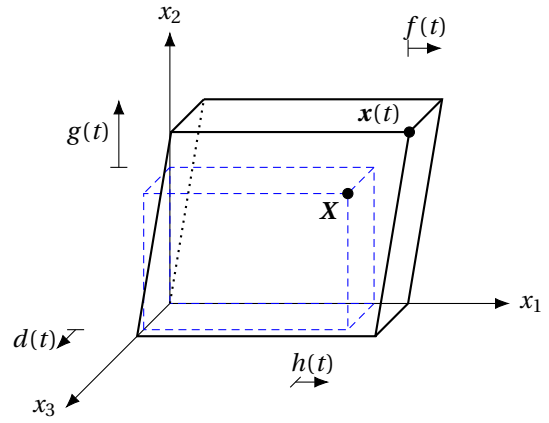


Figure 5. Kinematic of deformation in three dimensions

The objective stress rate is expressed by means of the Jaumann-Zaremba rate, Truesdell and Noll [1992]

$$\dot{\mathbf{T}} = \dot{\mathbf{T}} - \mathbf{W}\mathbf{T} + \mathbf{T}\mathbf{W} \quad , \quad (6)$$

where $\dot{\mathbf{T}}$ is the time derivative of the stress, $\dot{\mathbf{T}}$ is the objective stress rate from the constitutive relation and \mathbf{T} is the actual Cauchy-stress.

For the simple shear test with constant volume the homogeneous deformation is kinematically prescribed. Therefore the unknowns in the calculation are the time derivatives $\dot{f}(t)$, $\dot{g}(t)$, $\dot{h}(t)$ and $\dot{d}(t)$. They can be merged in the vector $\dot{\mathbf{a}}$

$$\dot{\mathbf{a}}(t) = \begin{bmatrix} \dot{f}(t) \\ \dot{g}(t) \\ \dot{h}(t) \\ \dot{d}(t) \end{bmatrix} \quad . \quad (7)$$

In stress controlled simulations for a given time step Δt the stress rate $\dot{\mathbf{T}}(t)$ is prescribed. For Hypoplasticity and Barodesy with the known actual stress state $\mathbf{T}(t)$ the deformation $\mathbf{a}(t)$ and its estimated time derivative $\dot{\mathbf{a}}$ yield the stress rate $\dot{\mathbf{T}}(\dot{\mathbf{a}})$. The vector $\dot{\mathbf{a}}(t)$ is determined with Newton's method.

The stress $\mathbf{T}(t)$ is given by (20) and the rotation angle $\theta = t\omega$, where ω is the angular velocity of the rotation. The rate of the deformation functions $\dot{\mathbf{a}}(t)$ is searched to determine the deformation. In each time step Δt from t_i to $t_i + \Delta t$ we know the stress rate

$$\dot{\mathbf{T}}(t_i) = \frac{\mathbf{T}(t_i + \Delta t) - \mathbf{T}(t_i)}{\Delta t} = \frac{\mathbf{T}_{i+1} - \mathbf{T}_i}{\Delta t} = \dot{\mathbf{T}}_i \quad (8)$$

and have to find the corresponding time rates of the deformation functions \dot{f} , \dot{g} , \dot{h} and \dot{d} from (4), which are collected in the vector $\dot{\mathbf{a}}$ (7). We employ Newton's method for this task and denote each iteration with the superscript (n) and each time step with the subscript i .

The first iteration $n = 0$ starts with an estimated $\dot{\mathbf{a}}_i^{(n)}$. With this estimation $\mathbf{D}(\dot{\mathbf{a}}_i^{(n)})$ and $\mathbf{W}(\dot{\mathbf{a}}_i^{(n)})$ are calculated with (4) and (5). At the beginning of the calculation $\mathbf{a}(t = 0) = \mathbf{0}$ holds. The stress rate $\dot{\mathbf{T}}_i^{(n)}$ is calculated by

$$\dot{\mathbf{T}}_i^{(n)} = \dot{\mathbf{T}}_i(\mathbf{T}_i, \mathbf{D}(\dot{\mathbf{a}}_i^{(n)}), \mathbf{E}_i) + \mathbf{W}(\dot{\mathbf{a}}_i^{(n)})\mathbf{T}_i - \mathbf{T}_i\mathbf{W}(\dot{\mathbf{a}}_i^{(n)}) \quad , \quad (9)$$

where E_i are internal variables at the beginning of the time step, e.g. the void ratio e_i . The residuum $R_i^{(n)}$ is the difference between the prescribed stress rate \dot{T}_i and the obtained stress rate $\dot{T}_i^{(n)}(\mathbf{D}(\dot{\mathbf{a}}_i^{(n)}), \mathbf{W}(\dot{\mathbf{a}}_i^{(n)}), \mathbf{T}_i, E_i)$ in the n^{th} iteration of the i^{th} time step. The new estimation of $\dot{\mathbf{a}}_i^{(n+1)}$ is calculated by

$$\dot{\mathbf{a}}_i^{(n+1)} = \dot{\mathbf{a}}_i^{(n)} - \left(\frac{\partial \dot{T}_i}{\partial \dot{\mathbf{a}}_i} (\dot{\mathbf{a}}_i^{(n)}) \right)^{-1} R_i^{(n)} . \quad (10)$$

If the norm of $R_i^{(n)}$ is smaller than a given tolerance, $\dot{\mathbf{a}}_i^{(n)}$ is accepted and a time integration with this $\dot{\mathbf{a}}_i$ is performed

$$\mathbf{a}_{i+1} = \mathbf{a}(t_{i+1}) = \mathbf{a}(t_i) + \dot{\mathbf{a}} \Delta t = \mathbf{a}_i + \dot{\mathbf{a}}_i \Delta t . \quad (11)$$

The deformation \mathbf{x}_{i+1} , the stress \mathbf{T}_{i+1} and the internal variables E_{i+1} follow in a similar way.

Since the deformation also contains a rotation, a time integration of the stretching in the form of $\boldsymbol{\varepsilon}_{i+1} = \boldsymbol{\varepsilon}_i + \mathbf{D}_i \Delta t$ is not correct. To get the correct logarithmic strain (also known as true or Hencky strain) in the reference configuration, the stretching has to be rotated back into this reference configuration. Hence, the true strain $\boldsymbol{\varepsilon}_{i+1}$ is calculated with \mathbf{D}_i (4)

$$\boldsymbol{\varepsilon}_{i+1} = \boldsymbol{\varepsilon}_i + \mathbf{Q}_i^T \mathbf{D}_i \mathbf{Q}_i \Delta t . \quad (12)$$

Here \mathbf{Q}_i is the rotation matrix of \mathbf{F}_i , where

$$\mathbf{F}_i = \frac{\partial \mathbf{x}}{\partial \mathbf{X}} = \mathbf{Q}_i \mathbf{U}_i = \mathbf{V}_i \mathbf{Q}_i . \quad (13)$$

In the case of Sanisand a different approach has to be used. Since in Sanisand, Taiebat and Dafalias [2008], the stretching \mathbf{D} is the dependent variable $\mathbf{D} = \mathbf{f}(\dot{\mathbf{T}}, \mathbf{T}, \dots)$, the objective stress rate $\dot{\mathbf{T}} \neq \dot{T}$, see (6), has to be determined with Newton's method.

Here the objective stress rate $\dot{\mathbf{T}}_i^{(n)}$ is estimated in the first iteration step. This results in a stretching tensor $\mathbf{D}_i^{(n)} = \mathbf{f}(\dot{\mathbf{T}}_i^{(n)}, \mathbf{T}_i, E_i)$ from which the components of $\dot{\mathbf{a}}_i^{(n)}$ can be calculated using

$$\dot{h}_i^{(n)} = D_{11}^{(n)} (1 + h_i) , \quad (14)$$

$$\dot{g}_i^{(n)} = D_{22}^{(n)} (1 + g_i) , \quad (15)$$

$$\dot{d}_i^{(n)} = D_{33}^{(n)} (1 + d_i) \quad \text{and} \quad (16)$$

$$\dot{f}_i^{(n)} = \frac{2D_{12}^{(n)} (1 + h_i)(1 + g_i) + \dot{h}_i^{(n)} f_i}{1 + h_i} . \quad (17)$$

With known $\dot{\mathbf{a}}_i^{(n)} = \mathbf{a}(\dot{\mathbf{T}}_i^{(n)})$ the spin tensor $\mathbf{W}_i^{(n)} = \mathbf{W}(\dot{\mathbf{a}}_i^{(n)}) = \mathbf{W}(\mathbf{a}(\dot{\mathbf{T}}_i^{(n)}))$ and the stress rate $\dot{\mathbf{T}}_i^{(n)}$ can be calculated with (5) and

$$\dot{\mathbf{T}}_i^{(n)} = \dot{\mathbf{T}}_i^{(n)} + \mathbf{W}_i^{(n)} \mathbf{T}_i - \mathbf{T}_i \mathbf{W}_i^{(n)} . \quad (18)$$

The new estimation for $\dot{\mathbf{T}}_i^{(n+1)}$ is calculated by

$$\dot{\mathbf{T}}_i^{(n+1)} = \dot{\mathbf{T}}_i^{(n)} - \left(\frac{\partial \dot{T}_i}{\partial \dot{\mathbf{T}}_i} (\dot{\mathbf{T}}_i^{(n)}) \right)^{-1} R_i^{(n)} . \quad (19)$$

Again, if the norm of the residuum $R_i^{(n)} = \dot{\mathbf{T}}_i^{(n)} - \dot{\mathbf{T}}_i$ is smaller than a given tolerance, $\dot{\mathbf{T}}_i^{(n)}$ and $\dot{\mathbf{a}}_i$ are accepted as solutions, we further proceed like for the other models.

4. Rotation of principal stresses with a $1\gamma 2\varepsilon$ apparatus

In this section, some results of tests with the $1\gamma 2\varepsilon$ apparatus, Joer et al. [1992] (schematic sketch in Fig. 6) are compared with numerical simulations with the above chosen constitutive models.

4.1. Testing device

The apparatus consists of a parallelogram (OABC), which encloses the sample. The parallelogram can undergo horizontal and vertical elongations and a shear deformation (tilting of sides AB and CO). The sides AO and BC remain horizontal and the sides AB and CO remain parallel during the deformation. Therefore, four motors are necessary, which control the elongations. The point O is fixed. Each side consists of six comb-shaped segments, interlocked in such a way that they maintain the continuity of the side.

The four sides are linked with hinges in such a way that they can be tilted. Shear strain is imposed by applying a horizontal displacement at the center of AB by a fifth motor, so that the side tilts around A and, correspondingly, the side CO around O.

The corners B, C and O are equipped with strain-gauged hinges consisting of two complete strain-gauge bridges placed inside a cylinder. This allows measurement of the forces applied at each corner in horizontal and vertical directions, Fig. 7. Assuming homogeneous stress in the sample, the stress state can be determined from the applied forces.

The deformation is controlled by the velocities imposed by the motors. Strain paths can be easily prescribed, since the deformation is controlled. In our case we have stress path control and this requires the use of servo-control, where the deformation is adjusted according to the measured forces.

Schneebeli cylinders of polyvinyl chloride (PVC) with different diameters (1.5, 3 and 3.5 mm), which can be seen as a two dimensional analogous material to soil, Schneebeli [1956], are used in these tests. Joer et al. [1998] give no further description of the material and its initial state at the test. Hence, it is not determinable if the sample was in a dense or loose state.

4.2. Stress path

The complex cyclic shear tests with constant principal stress values, Joer et al. [1998], are numerically simulated.

The sample is initially loaded with a vertical stress $\sigma_{22} = \sigma_{\max} = 90 \text{ kPa}$ and lateral stress $\sigma_{11} = \sigma_{\min} = 50 \text{ kPa}$. σ_{\max} , σ_{int} and σ_{\min} denote the maximum, intermediate and minimum principal stresses, respectively. The sample is deformed in a way that the directions of the principal stresses rotate while their values remain constant. This

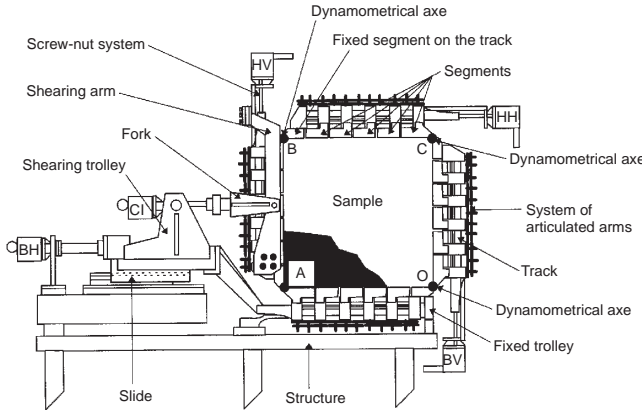


Figure 6. Schematic diagram of the $1\gamma 2\varepsilon$ apparatus (from Joer et al. [1998])

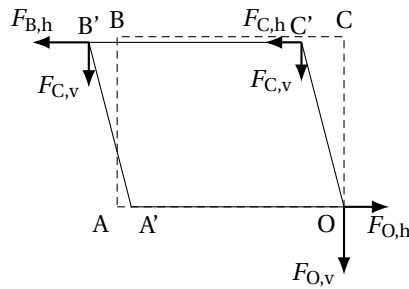


Figure 7. Deformed configuration of the $1\gamma 2\varepsilon$ apparatus with force measurements

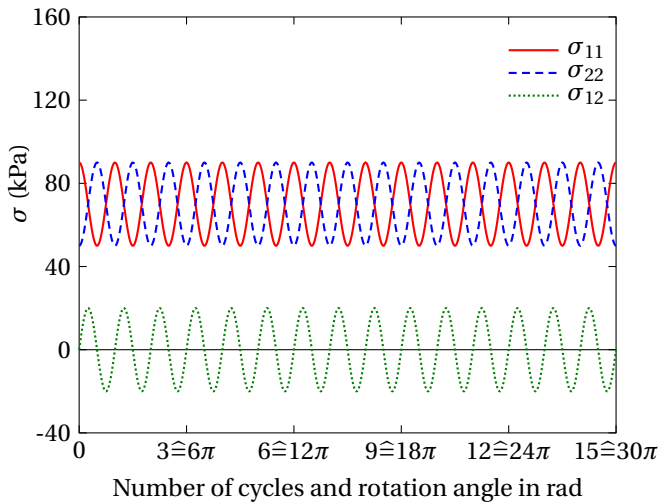


Figure 8. Prescribed stresses in the $1\gamma 2\varepsilon$ apparatus

stress evolution can be described by the following equations

$$\begin{aligned} \sigma_{11} &= \frac{\sigma_{\max} + \sigma_{\min}}{2} - \frac{\sigma_{\max} - \sigma_{\min}}{2} \cos\theta, \\ \sigma_{22} &= \frac{\sigma_{\max} + \sigma_{\min}}{2} + \frac{\sigma_{\max} - \sigma_{\min}}{2} \cos\theta \quad \text{and} \quad (20) \\ \sigma_{12} &= \frac{\sigma_{\max} - \sigma_{\min}}{2} \sin\theta \end{aligned}$$

(cf. Figure 8). θ denotes the angle of the rotation. Note that

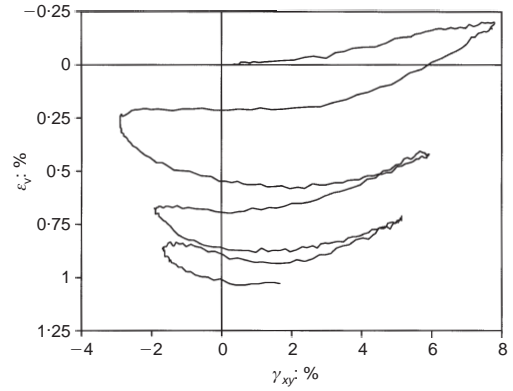


Figure 9. Volumetric strain vs. shear strain, experimental results, Joer et al. [1998]

the directions of the principal stresses σ_{\max} and σ_{\min} are variable, whereas the direction of σ_{int} is fixed and coincides with the x_3 -direction.

The numerical simulations are conducted as element tests. A further assumption has to be made for the boundary condition in the out of plane direction (x_3 in Fig. 5). The out of plane stress has to be constant to keep the invariants of the stress tensor constant. Starting from an isotropic stress state (mean effective stress $\sigma_{\max} = \sigma_{\text{int}} = \sigma_{\min} = 30$ kPa) the stress is anisotropically increased to $\sigma_{\max} = 90$ kPa and $\sigma_{\text{int}} = \sigma_{\min} = 50$ kPa.

The finite element program PLAXIS is used for the simulation of Hardening soil since this model is not explicitly published. All other calculations are conducted with MATLAB.

4.3. Results

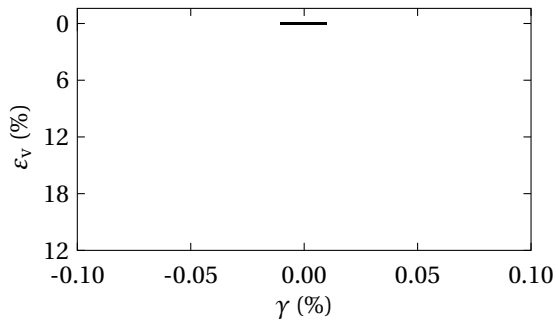
The volumetric strain ($\varepsilon_v = \varepsilon_{11} + \varepsilon_{22}$) is plotted versus the shear strain ($\gamma = 2\varepsilon_{12}$), Fig. 9. An overall decrease of the volume can be seen in the laboratory test.

The numerical results of the two elastoplastic constitutive models (Sanisand and Hardening Soil) are shown in Figure 10. The Hardening Soil Model (Fig. 10a) does not show any volumetric response. Contrary, Sanisand is able to reproduce the compaction qualitatively (Fig. 10b). Both hypoplastic and barodetic models are able to reproduce a compaction, Fig. 11 and 12. None of the models is able to reproduce the dilatation at the start of the test and at the end of each cycle.

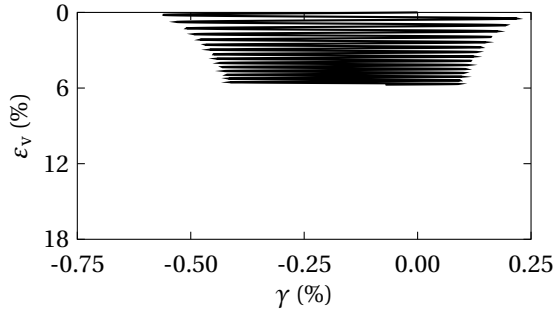
In Fig. 13 to 17 the volumetric and deviatoric strains are plotted versus the number of cycles. In these plots all strain components are considered, i.e. the volumetric strain is defined as $\varepsilon_v = \varepsilon_{11} + \varepsilon_{22} + \varepsilon_{33}$ and the deviatoric strain as $\varepsilon_q = \sqrt{\frac{3}{2} \text{tr} \mathbf{e}^2}$ with $\mathbf{e} = \boldsymbol{\varepsilon} - \frac{1}{3} \varepsilon_v \mathbf{I}$.

5. Rotation of principal stresses with a hollow cylinder apparatus

A rotation of principal stresses can also be applied in a hollow cylinder test (e.g. Broms and Casberian [1965], Ishihara and Towhata [1983], Miura et al. [1986], Tong et al. [2010], Yang et al. [2007]). A schematic sketch of a hollow cylinder

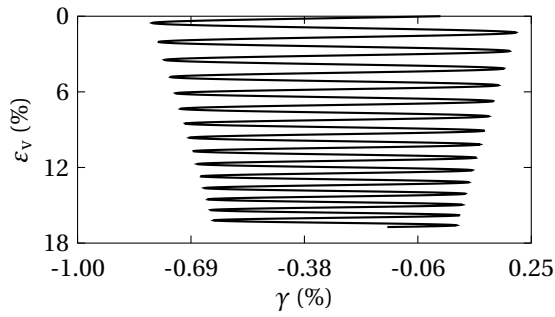


(a) Hardening Soil Small

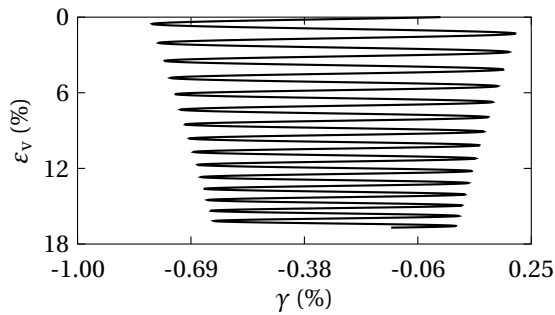


(b) Sanisand

Figure 10. Results of the simulation with the two elastoplastic constitutive models



(a) Hypo



(b) Hypo intergranular strain

Figure 11. Volumetric behaviour of Hypoplastic models

is shown in Fig. 18. The soil sample is loaded with an axial force, W , an inner pressure, p_i , an outer pressure, p_o and also a torque T .

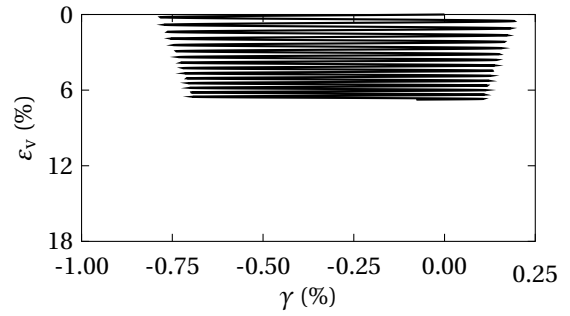


Figure 12. Volumetric behaviour of Barodesy

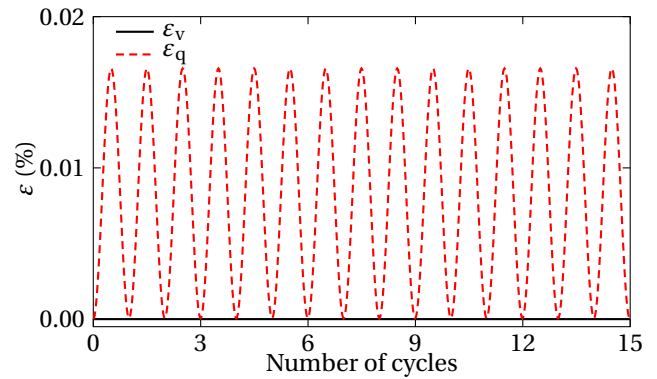


Figure 13. Volumetric and deviatoric strains in the $1\gamma 2\varepsilon$ -simulation with Hardening Soil Small

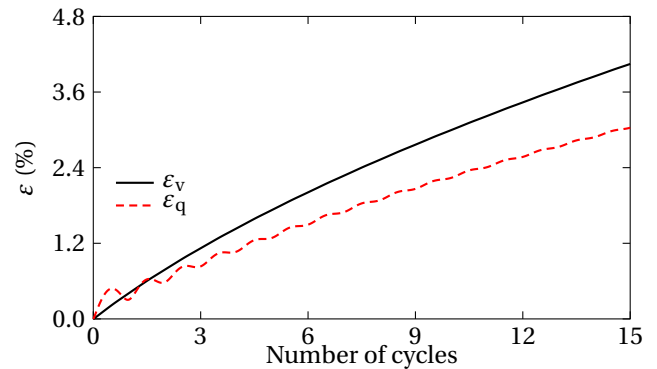


Figure 14. Volumetric and deviatoric strains in the $1\gamma 2\varepsilon$ -simulation with Sanisand

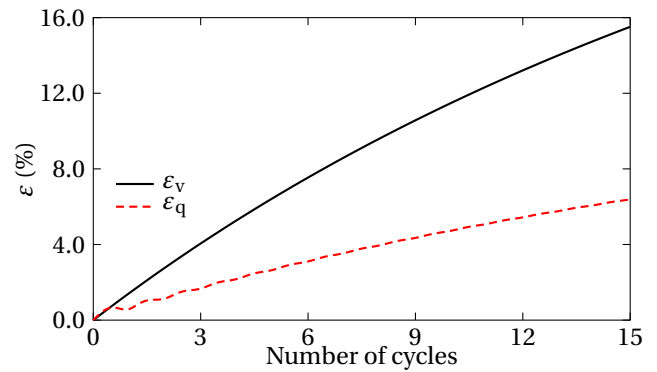


Figure 15. Volumetric and deviatoric strains in the $1\gamma 2\varepsilon$ -simulation with Hypo

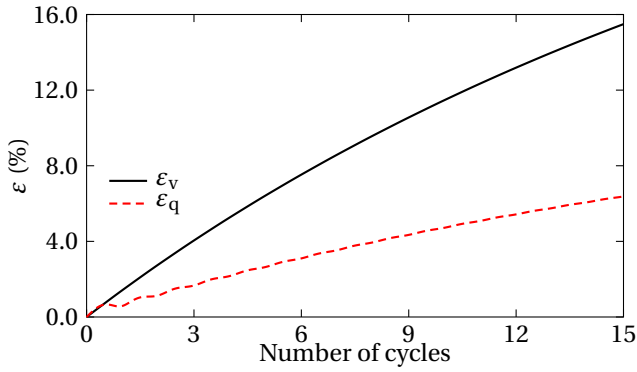


Figure 16. Volumetric and deviatoric strains in the $1\gamma 2\varepsilon$ -simulation with Hypo with intergranular strain

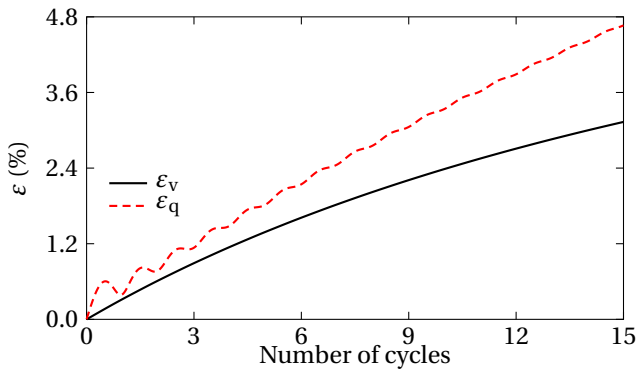


Figure 17. Volumetric and deviatoric strains in the $1\gamma 2\varepsilon$ -simulation with Barodesy

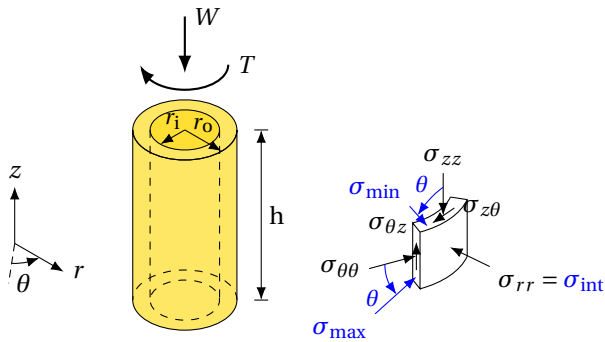


Figure 18. Schematic sketch of a hollow cylinder test

It is not possible to measure the stress in the sample directly and the stress is not constantly distributed in the specimen, e.g. for different inner and outer pressures the radial stress changes from p_i to p_o along the wall thickness. To compare the results of the laboratory test, averaged stresses are used. Hence, some assumptions on the stress distribution and the material behaviour are necessary. In the literature several solutions can be found, depending on whether the averaging of the stress is made over the thickness of the wall (e.g. Hight et al. [1983], Miura et al. [1986] and Yang et al. [2007]) or the volume (e.g. Naughton and O’Kelly [2007] and Sayao and Vaid [1991]), if it is assumed

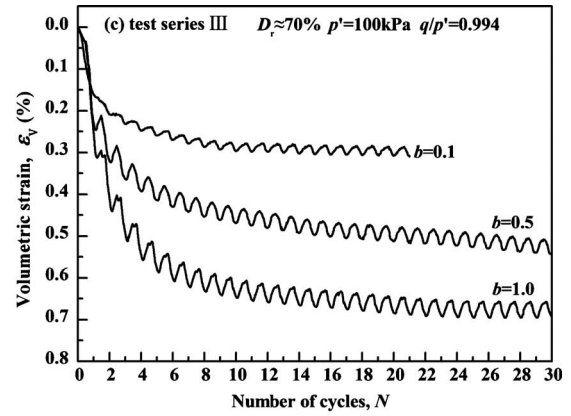


Figure 19. Volumetric strain vs. numbers of cycles in a hollow cylinder test with Toyoura Sand from Tong et al. [2010]

that the cylinder is thin-walled (Yang et al. [2007]) or thick-walled (Naughton and O’Kelly [2007]), or if the stresses are calculated for a linear elastic material (Hight et al. [1983]), partially plastic (Sayao and Vaid [1991]) or an average of elastic and plastic solutions (Yang et al. [2007]). In general, the differences of the averaged stresses are small for all different assumptions. The stresses in Tong et al. [2010] are calculated with the assumptions of a thin walled cylinder, linear elastic material behaviour and for the shear stress the average of the elastic and the plastic solution is used according to Yang et al. [2007].

The initial conditions are given as void ratio $e = 0.737 \pm 0.007$ ($D_r \approx (70 \pm 2)\%$), isotropic stress $p = 30$ kPa. The sample is then anisotropically compressed so that $\sigma_{\max} = 157.4$ kPa, $\sigma_{\text{int}} = 100$ kPa and $\sigma_{\min} = 42.6$ kPa. This results in a mean normal stress $p = 100$ kPa, a deviatoric stress $q = 99.4$ kPa and $b = 0.5$.⁽¹⁾ The result of the laboratory test is shown in Fig. 19.

The results of the simulations are shown in Figs. 20 to 24, where the development of volumetric strain ε_v and a measure for deviatoric strain ε_q with respect to the cycling is presented. All simulations except Hardening Soil show dilatation, which is opposite to the behaviour of the physical test. Hardening Soil shows, like in the $1\gamma 2\varepsilon$ test, no volumetric change. The evolutions of the deviatoric strains predicted by the models differ considerably, cf. Fig. 25. The deviatoric strains from the physical test have not been published and, thus, cannot be compared with the simulated ones. It is also conceivable that the elastic solution used for the evaluation of the physical tests is not valid.

Note that a recently published new version of Sanisand [Petalas et al., 2019] is able to predict the measured contractant behavior in the hollow cylinder test of Figs. 20 to 24. This model introduces additionally an anisotropic critical state line, a fabric tensor, a deviatoric plastic strain rate tensor, and effects of noncoaxiality are explicitly considered. Thus, this model ends up with 4 additional material parameters

$$^{(1)}q = \sqrt{[(\sigma_{\max} - \sigma_{\text{int}})^2 + (\sigma_{\text{int}} - \sigma_{\min})^2 + (\sigma_{\max} - \sigma_{\min})^2] / 2}$$

$$b = \frac{\sigma_{\text{int}} - \sigma_{\min}}{\sigma_{\max} - \sigma_{\min}}$$

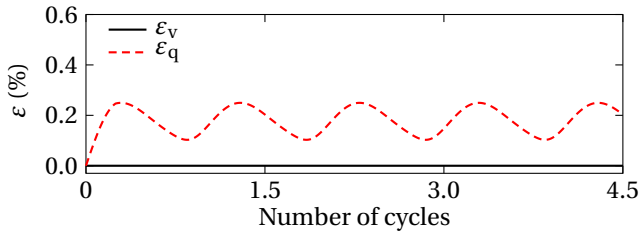


Figure 20. Volumetric and deviatoric strains in a hollow cylinder, numerical simulation with Hardening Soil

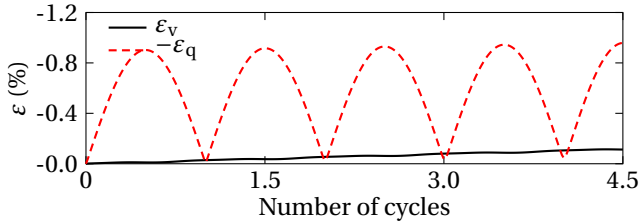


Figure 21. Volumetric and deviatoric strains in a hollow cylinder, numerical simulation with Sanisand

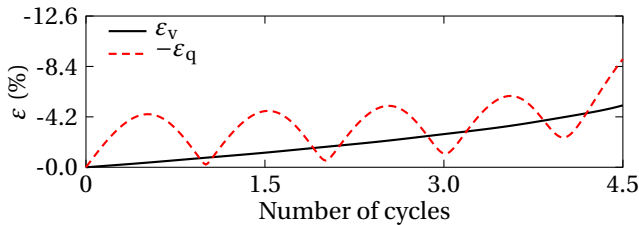


Figure 22. Volumetric and deviatoric strains in a hollow cylinder, numerical simulation with Hypoplasticity

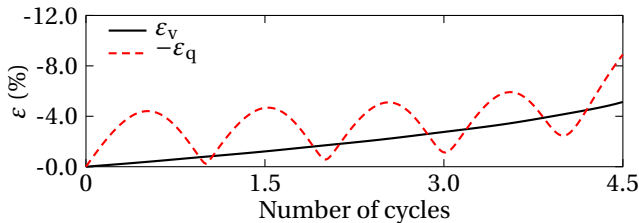


Figure 23. Volumetric and deviatoric strains in a hollow cylinder, numerical simulation with Hypoplasticity with intergranular strain

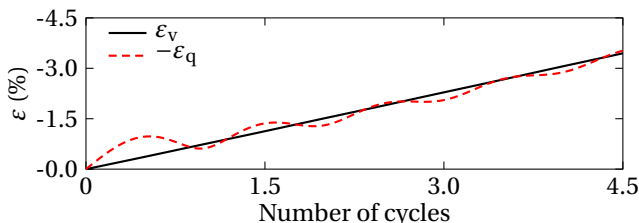


Figure 24. Volumetric and deviatoric strains in a hollow cylinder, numerical simulation with Barodesy

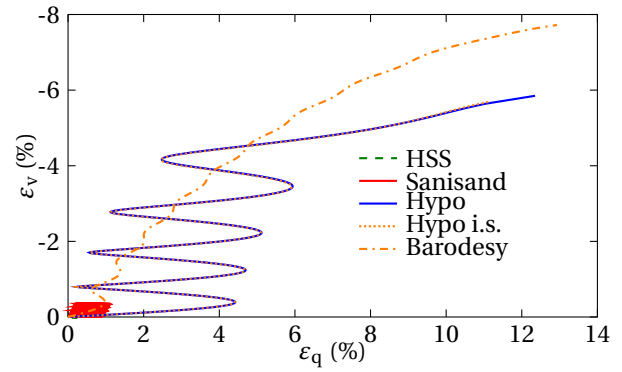


Figure 25. Deviatoric vs. volumetric strains for the different hollow cylinder simulations

(i.e. 20 parameters in total) and two tensors of internal state variables, for which the initial conditions have to be determined. This shows that the Sanisand-FN model is far more complex than the here employed Sanisand-model [Taiebat and Dafalias, 2008]. The other here used models have even less material parameters than this Sanisand-model (e.g. Barodesy with 7 material parameters), thus the new Sanisand-FN model is less comparable.

6. Conclusions

The volumetric changes of sand are mainly due to dilatancy (and contractancy). Dilatancy is an intricate property responsible for many important effects, such as liquefaction. However, both experimental observation and numerical simulation are difficult and prone to errors. The measurement of volumetric changes in experiments proves to be very sensitive, as different measurement methods (e.g. measurements of the boundary displacements vs. tomographic measurements) often deviate. Numerical simulations depend on the implementation of the critical void ratio and its dependence on stress, the experimental determination of which is very uncertain, Muir Wood [1990].

The simulation of tests with rotation of principal axes (shear tests) is a veritable extrapolation if the constitutive model has been calibrated on the basis of rectilinear extensions only. Clearly, extrapolations are more risky than other tests, which can be understood rather as interpolations. Correspondingly, a realistic simulation of shear tests is more difficult to achieve and cannot be expected from every constitutive model. It should also be taken into account that deviations from homogeneity are more pronounced in shear tests, and this makes such tests less appropriate for calibration and also for validation.

It can be seen from the numerical simulations that constitutive models which use only the principal stresses can, clearly, not reproduce the volumetric changes of soil due to principal stress rotation. This is shown here for the Hardening Soil model, but applies also for the often used simpler elastoplastic model with a Mohr-Coulomb failure criterion. In the case of elastoplastic models this shortcoming can be eliminated with a reformulation of the failure surface and flow rule in a six dimensional stress space as shown in

Ishihara and Towhata [1983]. The hypoplastic and barodetic models are able to reproduce a volumetric change without any further modification.

Advanced constitutive relations can model volumetric change of soil due to a rotation of the principal stresses. However, we have shown a case where these models predict a dilatant behaviour for this type of loading whereas the corresponding laboratory test shows contractant behaviour. Note that the used constitutive relations model the volumetric behaviour of drained triaxial and simple shear tests quite satisfactorily and similarly to each other. This discrepancy in the results of conventional laboratory tests and principal stress rotation experiments is a clear hint that further research is needed to obtain a reliable volumetric behaviour of constitutive models under complex stress paths. A successful example of such a development is the recently published Sanisand-FN model.

Acknowledgements

The authors are grateful to the two referees for their constructive and helpful comments on this paper.

Review History

This paper was sent to two Reviewers: David Mašin at the Charles University in Prague, and X. S. Shi at the Hong Kong University of Science and Technology. The two reviewers remained anonymous during the entire revision process. After the reviewing process was completed, both reviewers decided to disclose their identity. There was a single round of reviewing and correction after which both reviewers and the editor decided to accept the paper. Please see the Review History online for the complete reviews: ReviewHistory.pdf

References

- Arthur, J. R. F., Chua, K. S., Dunstan, T., and Rodriguez, J. I. (1980). Principal Stress Rotation: A Missing Parameter. *Journal of the Geotechnical Engineering Division, Proceedings of ASCE*, 106(4):419–433.
- Benz, T. (2007). *Small-strain stiffness of soils and its numerical consequences*. Number 55 in Mitteilung des Instituts für Geotechnik. IGS. Zugl.: Stuttgart, Univ., Diss., 2006.
- Broms, B. B. and Casberian, A. O. (1965). Effects of Rotation of the Principal Stress Axes and of the Intermediate Principal Stress on the Shear Strength. In *Proceedings of the Sixth International Conference on Soil Mechanics and Foundation Engineering*, volume I, pages 179–183. University of Toronto Press.
- Fellin, W. (2000). *Rütteldruckverdichtung als plastodynamisches Problem (Deep vibrocompaction as plastodynamic problem)*, volume 2 of *Advances in Geotechnical Engineering and Tunnelling*. Balkema.
- Gutierrez, M. and Ishihara, K. (2000). Non-coaxiality and energy dissipation in granular materials. *Soils and Foundations*, 40(2):49–59.
- Gutierrez, M., Ishihara, K., and Towhata, I. (1991a). Flow theory for sand during rotation of principal stress direction. *Soils and Foundations*, 31(4):121–132.
- Gutierrez, M., Ishihara, K., and Towhata, I. (1991b). Modelling the Deformation of Sand during Cyclic Rotation of Principal Stress Directions. In *International Conferences on Recent Advances in Geotechnical Earthquake Engineering and Soil Dynamics*, pages 7–12. University of Missouri–Rolla.
- Gutierrez, M., Ishihara, K., and Towhata, I. (1993). Model for the deformation of sand during rotation of principal stress directions. *Soils and Foundations*, 33(3):105–117.
- Gutierrez, M. and Vardoulakis, I. (2007). Energy dissipation and post-bifurcation behaviour of granular soils. *International Journal for Numerical and Analytical Methods in Geomechanics*, 31(3):435–455.
- Gutierrez, M. and Wang, J. (2009). Non-coaxial version of Rowe's stress-dilatancy relation. *Granular Matter*, 11(2):129–137.
- Gutierrez, M., Wang, J., and Yoshimine, M. (2009). Modeling of the simple shear deformation of sand: effects of principal stress rotation. *Acta Geotechnica*, 4(3):193–201.
- Herle, I. (1997). *Hypoplastizität und Granulometrie einfacher Korngerüste*, volume 142 of *Veröffentlichung des Institutes für Bodenmechanik und Felsmechanik*. Karlsruhe: Inst. für Bodenmechanik und Felsmechanik.
- Hight, D. W., Gens, A., and Symes, M. J. (1983). The development of a new hollow cylinder apparatus for investigating the effects of principal stress rotation in soils. *Géotechnique*, 33(4):355–383.
- Ishihara, K. and Towhata, I. (1983). Sand response to cyclic rotation of principal stress directions as induced by wave loads. *Soils and Foundations*, 23(4):11–26.
- Joer, H., Lanier, J., Desrues, J., and Flavigny, E. (1992). "1 γ 2 ϵ ": A New Shear Apparatus to Study the Behavior of Granular Materials. *Geotechnical Testing Journal*, 15(2):129–137.
- Joer, H., Lanier, J., and Fahey, M. (1998). Deformation of granular materials due to rotation of principal axes. *Géotechnique*, 48(5):605–619.
- Kolymbas, D. (1985). A generalized hypoelastic constitutive law. In *Proc. XI Int. Conf. Soil Mechanics and Foundation Engineering, San Francisco*, volume 5, page 2626. Balkema.
- Kolymbas, D. (1991). An outline of hypoplasticity. *Archive of Applied Mechanics*, 61(3):143–151.
- Kolymbas, D. (2012). Barodesy: a new constitutive frame for soils. *Géotechnique Letters*, 2:17–23.
- Kolymbas, D. (2015). Introduction to barodesy. *Géotechnique*, 65(1):52–65.
- Miura, K., Miura, S., and Toki, S. (1986). Deformation behavior of anisotropic dense sand under principal stress axes rotation. *Soils and Foundations*, 26(1):36–52.
- Muir Wood, D. (1990). *Soil Behaviour and Critical State Soil Mechanics*. Cambridge University Press.
- Naughton, P. J. and O'Kelly, B. C. (2007). Stress non-uniformity in a hollow cylinder torsional sand specimen. *Geomechanics and Geoengineering*, 2(2):117–122.
- Niemunis, A. and Herle, I. (1997). Hypoplastic model for cohesionless soils with elastic strain range. *Mechanics of Cohesive-frictional Materials*, 2(4):279–299.

- Petalas, A. L., Dafalias, Y. F., and Papadimitriou, A. G. (2019). SANISAND-FN: An evolving fabric-based sand model accounting for stress principal axes rotation. *International Journal for Numerical and Analytical Methods in Geomechanics*, 43(1):97–123.
- Pradel, D., Ishihara, K., and Gutierrez, M. (1990). Yielding and flow of sand under principal stress axes rotation. *Soils and Foundations*, 30(1):87–99.
- Sayao, A. and Vaid, Y. P. (1991). A critical assessment of stress nonuniformities in hollow cylinder test specimens. *Soils and Foundations*, 31(1):60–72.
- Schneebeli, G. (1956). Une analogie mécanique pour les terres sans cohésion. *Comptes rendus hebdomadaires des séances de l'Académie des sciences*, 243:125–126.
- Schwiteilo, E. and Herle, I. (2017). Vergleichsstudie zur Kompressibilität und zu den Scherparametern von Ton aus ödometer- und Rahmenscherversuchen. *geotechnik*, 40(3):204–217.
- Taiebat, M. and Dafalias, Y. F. (2008). SANISAND: Simple anisotropic sand plasticity model. *International Journal for Numerical and Analytical Methods in Geomechanics*, 32(8):915–948.
- Tong, Z.-X., Zhang, J.-M., Yu, Y.-L., and Zhang, G. (2010). Drained Deformation Behavior of Anisotropic Sands during Cyclic Rotation of Principal Stress Axes. *Journal of Geotechnical and Geoenvironmental Engineering*, 136(11):1509–1518.
- Truesdell, C. and Noll, W. (1992). *The Non-Linear Field Theories of Mechanics*. Springer, 2 edition.
- Verdugo, R. and Ishihara, K. (1996). The Steady State of Sandy Soils. *Soils and Foundations*, 36(2):81–91.
- von Wolffersdorff, P.-A. (1996). A hypoplastic relation for granular materials with a predefined limit state surface. *Mechanics of Cohesive-frictional Materials*, 1(3):251–271.
- Yang, Z. X., Li, X. S., and Yang, J. (2007). Undrained anisotropy and rotational shear in granular soil. *Géotechnique*, 57(4):371–384.

Manuscript received 5th June 2019, revised 19th September 2019, accepted 14th October 2019.